Renormalization-group study of Bose polarons

Felipe Isaule, Ivan Morera, Pietro Massignan, and Bruno Juliá-Díaz

Renormalization group study of Bose polarons

Felipe Isaule,[1] Ivan Morera,[1] Pietro Massignan,[2] and Bruno Juliá-Díaz[1]

[1]*Departament de Física Quàntica i Astrofísica, Facultat de Física, and Institut de Ciències del Cosmos (ICCUB), Universitat de Barcelona, Martí i Franquès 1, E–08028 Barcelona, Spain*

[2]*Departament de Física, Universitat Politècnica de Catalunya, Campus Nord B4-B5, E-08034 Barcelona, Spain*

(Dated: July 26, 2021)

We study the properties of a single impurity in a dilute Bose gas, a Bose polaron, using the functional renormalization group. We use an ansatz for the effective action motivated by a derivative expansion, and we compute the energies of the attractive and repulsive branches of excitations in both two and three spatial dimensions. Three-body correlations play an important role in the attractive branch, and we account for those by including three-body couplings between two bath bosons and the impurity. Our calculations compare very favorably with state-of-the-art experimental measurements and numerical simulations.

I. INTRODUCTION

The study of an impurity immersed in a quantum medium has a long history, dating back to the work of Landau and Pekar on electrons coupled to an ionic crystal [1]. Such impurity is understood as a dressed quasiparticle referred to as a polaron. Impurities in bosonic baths have been studied in a variety of configurations and played a key role in elucidating the physics of helium liquids [2, 3]. The polaron problem has been extensively studied also in fermionic mediums, particularly in condensed matter physics [4] and ultracold atoms [5–16].

The interest in an impurity immersed in a weakly interacting Bose gas, the Bose polaron, has greatly increased in the past decade. Indeed, the experimental progress in cold atom gases [17] has recently allowed the experimental realization of Bose polarons, including the regime of resonant boson-impurity interactions [18–21]. Theoretically, early perturbative works were restricted to the regime of weak boson-impurity interactions [22–24]. Improved descriptions emerged in recent years with a variety of techniques, including field theory approaches [25–29], variational methods [30–41], the Fröhlich model [42–44], and Monte Carlo (MC) simulations [45–49].

In the case of Bose polarons, the bosonic nature of the medium means that three- and more-body interactions can be important [32], and that the mixture is generally highly unstable against three-body losses. In contrast, in the case of Fermi polarons, interactions beyond the two-body level are suppressed by Pauli blocking, and the mixture is relatively long-lived. These differences make the theoretical description and experimental investigation of Bose polarons much more challenging. Furthermore, in a bosonic bath the dressed impurity has the same quantum statistics in the two asymptotic limits of zero and infinite attraction, so that the problem features a smooth polaron-to-molecule crossover [25]. In contrast, in a fermionic medium, a bare impurity and the molecule it forms by binding to a bath fermion have opposite quantum statistics, and therefore the spectrum of a Fermi polaron generally features a sharp polaron-to-molecule transition.

In this work we study Bose polarons using the functional renormalization group (FRG) based on the effective average action [50, 51] (for a complete review see Ref. [52]). The FRG is a non-perturbative field theory approach which proved to be a powerful tool to study strongly correlated systems, including Efimov physics in three-body [53–55] and four-body [56–59] systems, the BCS-BEC crossover [60–68], and the Fermi polaron [69–71] (for applications in other areas of physics see Refs. [51, 52]). The FRG permits to include systematically the effect of fluctuations, such as those arising from three- and more-body correlations, and to add their effect non-perturbatively over a wide range of scales. In addition, the FRG already provided accurate descriptions of Bose gases in two and three dimensions [72–78], including critical phenomena at the superfluid phase transitions [79]. Therefore, the FRG appears as a good technique to study novel physics in Bose polarons. Furthermore, because the FRG provides a unified description of few- and many-body physics within the same theory, studying polaron physics with FRG can provide important insight into Bose-Bose and Bose-Fermi mixtures.

In this article, we focus on Bose polarons at zero temperature in two and three spatial dimensions. We approximate the coarse-grained effective action under a derivative expansion, and we consider up to three-body correlations. Our approximation enables us to give a good description of the ground state energies and to quantify the importance of three-body forces. The article is organized as follows. In Sec. II we present our model and introduce the FRG flow equation. In Sec. III we study the repulsive branch of the Bose polaron, presenting the main aspects of our FRG calculations, as well as results for the polaron energy. In Sec. IV we study the attractive branch, stressing the specific considerations for the study of attractive interactions, and presenting results for the polaron energy with and without three-body correlations. In Sec. V we present the conclusions and outlook of our work. Finally, in Appendixes A and B we provide specific details of the RG equations, and in Appendix C we provide an estimation for the effective mass in the repulsive branch.

II. MODEL AND FRG EQUATION

We consider an impurity of mass m_I and energy μ_I immersed in a gas of weakly repulsive bosons of mass m_B and chemical potential μ_B. We approximate the boson-boson and boson-impurity interactions with contact potentials of strength g_{BB} and g_{BI}, respectively. In a field theory formulation, such system is described by the microscopic action [25]

$$
\mathcal{S}[\boldsymbol{\varphi}] = \int_x \left[\psi_B^\dagger \left(\partial_\tau - \frac{\nabla^2}{2m_B} - \mu_B \right) \psi_B \right.
$$
$$
+ \psi_I^\dagger \left(\partial_\tau - \frac{\nabla^2}{2m_I} - \mu_I \right) \psi_I
$$
$$
\left. + \frac{g_{BB}}{2}(\psi_B^\dagger \psi_B)^2 + g_{BI}\psi_B^\dagger \psi_I^\dagger \psi_B \psi_I \right], \quad (1)
$$

where we use natural units $\hbar = 1$, and $\int_x = \int_0^\infty d\tau \int d\mathbf{x}$, with $\tau = it$ the imaginary time. The microscopic action defines the grand-canonical partition function [51], and is a functional of the complex fields ψ_B and ψ_I, which represent the bath bosons and the impurity, respectively. Since we consider a single impurity, the quantum statistics of ψ_I is irrelevant.

The boson-boson interaction needs to be repulsive, in order to prevent the collapse of the bosonic medium. In contrast, the boson-impurity interaction can either be repulsive or attractive, leading to the repulsive and attractive branches of the Bose polaron. The repulsive branch is generally well described by perturbative approaches. In contrast, the attractive branch is more challenging to describe and shows richer physics. In particular, for strong attractive coupling the scattering length diverges in three dimensions, so that usual perturbative approaches may not be employed. Furthermore, three- and more-body physics can become important in the regime of strong coupling [32]. Therefore, more robust approaches have to be employed in this regime [34]. An analytic solution for the case of heavy polarons at unitarity was recently put forward in Ref. [38].

In this work, we extract the ground state properties of the Bose polaron from the Green's functions [25]. These can be obtained from $\mathcal{S}$ by taking into account all the quantum paths using the *path integral* formalism. However, it is more convenient to work in terms of the Legendre-transformed effective action Γ. The effective action is defined in terms of classical fields, and thus it already contains the effect of fluctuations. The Green's functions are then naturally obtained from the vertex functions $\Gamma^{(n)}$ (for details see Ref. [51]).

The effective action can be calculated perturbatively from a loop expansion. However, this is impractical in the regime of strong coupling, where one needs to take into account fluctuations over a wide range of scales. Within the functional renormalization group (FRG), the calculation of Γ is instead performed non-perturbatively. In this framework, a regulator function $\mathbf{R}_k$ is added to the

theory to suppress fluctuations at momenta $q \lesssim k$, so one works in terms of a k-dependent effective action Γ_k. At a high scale in the ultraviolet (UV) $k = \Lambda$, *all* fluctuations are suppressed and the effective action is simply the microscopic action $\Gamma_\Lambda = \mathcal{S}$. On the other hand, for $k \to 0$ all fluctuations are considered, and Γ_0 is the full effective action.

The flow of Γ_k as a function of k is dictated by the Wetterich equation [50]

$$
\partial_k \Gamma_k = \frac{1}{2} \operatorname{tr} \left[(\mathbf{\Gamma}_k^{(2)} + \mathbf{R}_k)^{-1} \partial_k \mathbf{R}_k \right], \quad (2)
$$

where $\mathbf{\Gamma}_k^{(2)}$ is the matrix with the second functional derivatives of Γ_k,

$$
\mathbf{\Gamma}_k^{(2)} = \frac{\delta^2 \Gamma_k}{\delta \boldsymbol{\varphi}_{-q}^\dagger \delta \boldsymbol{\varphi}_q}, \quad (3)
$$

and tr denotes both a matrix trace and an integral over internal momentum $q = (\omega, \mathbf{q})$. The Wetterich equation has a one loop structure with a propagator $\mathbf{G}_k = (\mathbf{\Gamma}_k^{(2)} + \mathbf{R}_k)^{-1}$, and insertion $\partial_k \mathbf{R}_k$ [50].

In most applications, one solves the RG flow by proposing an ansatz for Γ_k, which respects the symmetries of the microscopic theory. In this work we employ an ansatz based on a derivative expansion (DE) truncated to a small number of k-dependent couplings [52]. Within the DE, we expand the effective action up to a chosen number of fields and derivatives, and so the Wetterich equation becomes a set of coupled differential equations for the k-dependent couplings in the expansion. These equations can then be solved numerically using standard methods.

It has been shown that the DE gives an accurate description of various properties of the Fermi polaron in both two [71] and three [69] dimensions, including the onset of the polaron and molecule phases and their respective energies. Similarly, in this work we show that the DE provides a precise description of the ground state energy of the Bose polaron and also enables us to quantify the importance of three-body correlations.

In the following, we present the study of the repulsive and attractive branches separately. We start in Sec. III with the simpler repulsive branch to easily introduce our formalism. We then generalize our formalism to the attractive branch in Sec. IV.

III. REPULSIVE BOSE POLARONS

We start from action (1), and we neglect the feedback of the impurity on the medium. To solve the RG flow of the effective action in presence of repulsive impurity-bath interactions, we propose the following ansatz

$$
\Gamma_k[\boldsymbol{\varphi}] = \int_x \left[\psi_B^\dagger \left(S_B \partial_\tau - \frac{Z_B}{2m_B}\nabla^2 - V_B \partial_\tau^2 \right) \psi_B \right.
$$
$$
\left. + \psi_I^\dagger \left(S_I \partial_\tau - \frac{Z_I}{2m_I}\nabla^2 \right) \psi_I + U(\rho_B, \rho_I) \right], \quad (4)
$$

where S_B, Z_B, V_B, S_I, and Z_I are renormalization factors which we assume as field-independent, and

$$U = -P + u_I \rho_I + \frac{\lambda_{BB}}{2}(\rho_B - \rho_0)^2 + \lambda_{BI}(\rho_B - \rho_0)\rho_I \,, \quad (5)$$

is the effective potential expanded up to fourth-order in the fields, where $\rho_a = \psi_a^\dagger \psi_a$ ($a = B, I$), P is the pressure of the bath, u_I is a one-body coupling for the impurity, and λ_{BB} and λ_{BI} are the couplings associated to the boson-boson and boson-impurity interactions, respectively. All the couplings in the expansion, S_B, Z_B, V_B, S_I, Z_I, P, u_I, λ_{BB}, λ_{BI}, as well as the order parameter $\rho_0 = \langle \rho_B \rangle$, flow with k. We note that three- and more-body correlations are not important in the repulsive branch, and thus ansatz (4) only contains two-body couplings.

Our ansatz is based on the one used to study repulsive Bose-Bose mixtures [78], adapted to the limit of extreme population imbalance. The term $V_B \partial_\tau^2$ is necessary to correctly describe the bosonic medium in the infrared where the effective action develops phonons with linear dispersion, taking the form of a relativistic model [73]. An analogous term is not needed for the impurity, as the latter is not condensed.

We stress that our ansatz is only accurate for two- and three-dimensional gases. In one dimension, our level of truncation is not able to accurately capture the quasicondensate nature of the bath [72], where we have to carefully treat the stronger impact of phase fluctuations [77].

The minimum ρ_0 of the effective potential corresponds to the condensate density of the medium, giving its physical value at $k = 0$. If $\rho_0 > 0$, the $U(1)$-symmetry of the bosonic bath is broken, and the gas is condensed. Here we study the two- and three-dimensional polaron at zero temperature, so that ρ_0 is always non-zero. In contrast, for the impurity $\langle \rho_I \rangle = 0$. Furthermore, the superfluid density is given by the value at $k = 0$ of the superfluid stiffness $\rho_s = Z_B \rho_0$ [76]. Because at zero temperature all bosons are superfluid, we can extract the density of the medium n from $n = \rho_s$ [74]. We note that interactions deplete the condensate, $\rho_0 \leq \rho_s = n$, and therefore the mass renormalization coefficient Z_B flows to a value larger than unity for $k \to 0$ [74].

To solve the RG flow we need an equation for each running coupling. We obtain the flow equations from the Wetterich equation (2). These can be found in App. A. In addition, we need to choose a regulator. In this work, we use the optimized Litim regulator [80]

$$R_{k,a} = \frac{Z_a}{2m_a}(k^2 - \mathbf{q}^2)\Theta(k^2 - \mathbf{q}^2)\,, \qquad a = B, I \quad (6)$$

where Θ is the Heaviside step function. This choice enables us to perform the momentum integrals analytically before solving the RG flow. Finally, we need to specify the initial conditions of the RG flow. We do so in the following subsection.

A. Initial conditions of the RG flow

The RG flow is started at a scale $k = \Lambda$ much larger than the relevant scale of the bath, which in this case is given by the healing scale $k_h = (2m_B \mu_B)^{1/2}$ [74, 77]. At this high scale, we can impose that $\Gamma_\Lambda = \mathcal{S}$. We obtain

$$S_B(\Lambda) = Z_B(\Lambda) = S_I(\Lambda) = Z_I(\Lambda) = 1\,, \quad V_B(\Lambda) = 0\,,$$

$$\rho_0(\Lambda) = \frac{\mu_B}{\lambda_{BB}(\Lambda)}\,, \quad u_I(\Lambda) = -\mu_I + \mu_B\frac{\lambda_{BI}(\Lambda)}{\lambda_{BB}(\Lambda)}\,, \quad (7)$$

where $\mu_B > 0$, and $\mu_I/\mu_B < \lambda_{BI}(\Lambda)/\lambda_{BB}(\Lambda)$.

To connect the flow to known physical observables, we impose that the couplings λ_{BB} and λ_{BI} in vacuum ($\mu_B = \mu_I = 0$) correspond to the known two-body T-matrices at the physical limit $k = 0$ (see details in Ref. [74]). With this, the initial conditions for λ_{BB} and λ_{BI} depend on the boson-boson and boson-impurity scattering lenths a_{BB} and a_{BI}, respectively. For the optimized regulator (6), we have the same initial conditions as those for the repulsive Bose-Bose mixtures studied in Ref. [78]. These are

$$\lambda_\alpha(\Lambda) = \begin{cases} \dfrac{2\pi/m_\alpha}{1 - 2\gamma_E - \ln(a_\alpha^2 \Lambda^2/4)} & : d = 2 \\[2mm] \left(\dfrac{m_\alpha}{2\pi a_\alpha} - \dfrac{m_\alpha}{3\pi^2}\Lambda\right)^{-1} & : d = 3 \end{cases}, \quad (8)$$

where $\alpha = BB, BI$, and $\gamma_E \approx 0.577$ is the Euler-Mascheroni constant. The reduced masses are $m_{BB} = m_B/2$ and $m_{BI} = m_r = m_B m_I/(m_B + m_I)$. For purely repulsive potentials, the scattering lengths provide a lower bound to the potential ranges. Thus, a contact potential approximation becomes invalid for momenta larger than the inverse scattering length [77, 78]. The flow must therefore be restricted to $\Lambda < \min(a_{BI}^{-1}, a_{BB}^{-1})$. Nevertheless, we stress that because the interactions are renormalized by Eq. (8), as long as $\Lambda \gg k_h$ the results are independent of the choice of Λ. For more details see Refs. [74, 77].

The initial conditions completely define the RG flow in terms of the physical inputs μ_B, a_{BB} and a_{BI}, and the self-consistently determined μ_I. We then follow the RG flow by solving the flow equations of all the couplings. Note that we choose values of a_{BB} and μ_B which give the desired physical density of the bath for $k \to 0$ [74]. Examples of flows are given in App. A.

B. Propagator and polaron energy

As explained in Sec. II, the propagator of the FRG equation is given by $\mathbf{G}_k = (\Gamma_k^{(2)} + \mathbf{R}_k)^{-1}$. In momentum space $q = (\omega, \mathbf{q})$, the inverse propagator for ansatz (4) reads

$$\mathbf{G}_k^{-1}(q) = \begin{pmatrix} \mathbf{G}_{k,B}^{-1}(q) & \mathbf{0} \\ \mathbf{0} & \mathbf{G}_{k,I}^{-1}(q) \end{pmatrix}, \quad (9)$$

where

$$\mathbf{G}_{k,B}^{-1}(q) = \begin{pmatrix} E_{1,k}(\mathbf{q};\rho_B) + V_B\omega^2 & S_B\omega \\ -S_B\omega & E_{2,k}(\mathbf{q};\rho_B) + V_B\omega^2 \end{pmatrix}, \quad (10)$$

is the inverse propagator of the Bose gas, with

$$E_{1,k}(\mathbf{q};\rho_B) = E_{2,k}(\mathbf{q};\rho_B) + 2\rho_B U_B''(\rho_B), \quad (11)$$

$$E_{2,k}(\mathbf{q};\rho_B) = Z_B \frac{\mathbf{q}^2}{2m_B} + U_B'(\rho_B) + R_{k,B}(\mathbf{q}), \quad (12)$$

where the primes in U' and U'' indicate derivatives with respect to ρ_B, whereas

$$\mathbf{G}_{k,I}^{-1}(q) = \begin{pmatrix} E_{I,k}(\mathbf{q};\rho_B) + iS_I\omega & 0 \\ 0 & E_{I,k}(\mathbf{q};\rho_B) - iS_I\omega \end{pmatrix}, \quad (13)$$

is the inverse propagator of the impurity, with

$$E_{I,k}(\mathbf{q};\rho_B) = Z_I \frac{\mathbf{q}^2}{2m_I} + \partial_{\rho_I} U(\rho_B,\rho_I) + R_{k,I}(\mathbf{q}). \quad (14)$$

Note that we introduced real orthogonal fields $\psi_B = (\psi_{B,1}(x) + i\psi_{B,2}(x))/\sqrt{2}$, and evaluated all the fields at their background values $\psi_{B,1} = \sqrt{2\rho_B}\delta(q)$ and $\psi_{B,2} = \psi_I = \phi = 0$ [74].

The polaron energy μ_I corresponds to the energy needed to add an impurity to the medium. In the ground state, the Green's function of the impurity $\mathbf{G}_I$ (or analogously, the spectral function) has a pole at μ_I [25]. In our FRG formalism, we find the ground state energy by determining the energy μ_I that gives $\det(\mathbf{G}_{k,I}^{-1}(0)) = 0$ for $k \to 0$ [69].

From Eq. (13), by taking $\det(\mathbf{G}_{k,I}^{-1}) = 0$ at the minimum $\rho_B = \rho_0$, we find the pole

$$q_0^*(\mathbf{q}) = E_{I,k}(\mathbf{q})/S_I, \quad (15)$$

where $E_{I,k}$ is defined in Eq. (14). At zero momentum, $q_0^*(\mathbf{0}) = u_I/S_I$. Therefore, the physical polaron energy μ_I^* corresponds to the choice of μ_I which gives $q_0^*(\mathbf{0}) \to 0$ for $k \to 0$. Values of μ_I that do not fulfill this condition are not physical. An analogous condition is imposed to find the ground state of the Fermi polaron [69], and binding energies in few bosons problems [55]. We note that because in the DE we follow the flow at zero momentum $q = 0$ (see App. A), we can not study the poles at finite momenta in the current work.

C. Results

Following the approach sketched above, here we present results for the polaron energy for a range of boson-impurity scattering lengths a_{BI}. This scattering length can be tuned experimentally through Feshbach resonances [19]. We present results in both two and three dimensions and compare them with known results to check the robustness of our approach.
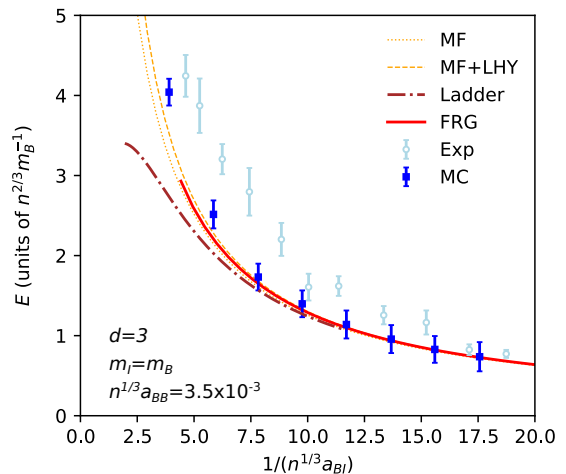

FIG. 1. Polaron energy E of the repulsive branch in three dimensions as a function of $(n^{1/3}a_{BI})^{-1}$. The solid red line corresponds to FRG calculations. The dash-dotted brown line corresponds to ladder calculations from Ref. [26]. The thin orange lines correspond to the perturbative solution (16) at the MF level (dotted) and with the LHY-type correction (dashed). The light blue open circles are experimental data from Ref. [47], and the blue squares are MC simulations from Ref. [47]. In all cases, $m_B = m_I$ and $n^{1/3}a_{BB} = 3.5 \times 10^{-3}$.

First, we show results in three dimensions in Fig. 1. We employ parameters that simulate the conditions of the Aarhus experiment [19], and scattering lengths $a_{BI} > a_{BB}$ so the effect of the boson-impurity interaction is important. We compare with MC simulations and experimental data from Ref. [47], ladder calculations from Ref. [26], and with the perturbative solution [81, 82]

$$E = \frac{2\pi a_{BI}n}{m_R}\left[1 + \frac{24}{3\sqrt{\pi}}\frac{m_R}{m_I}\sqrt{na_{BB}^3}\frac{a_{BI}}{a_{BB}}I(\gamma)\right], \quad (16)$$

where n is the density of the bosonic bath, $\gamma = m_B/m_I$, and

$$I(\gamma) = \frac{1+\gamma}{\gamma}\int_0^\infty dk\left[1 - \frac{(1+\gamma)k^2}{\sqrt{1+k^2}(\sqrt{1+k^2}+\gamma k)}\right],$$

which for equal masses takes the value $I(1) = 8/3$. The first term in Eq. (16) corresponds to the mean field (MF) solution, whereas the second term is a Lee-Huang-Yang (LHY) type correction.

We obtain a good agreement between our results and both the MC simulations and perturbative solutions. This is in line with previous FRG results for repulsive Bose-Bose mixtures [78]. We stress that the MC simulations include fluctuations at all orders, and thus they are a good benchmark for our calculations. We restrict our calculations to $(n^{1/3}a_{BI})^{-1} \gtrsim 4$, as for stronger boson-impurity interactions we have that $k_h \gtrsim a_{BI}^{-1}$, and thus we can not choose a sufficiently large value for the initial scale Λ [see discussion after Eq. (8)].

We show an analogous calculation in two dimensions in Fig. 2. We employ conditions that have been
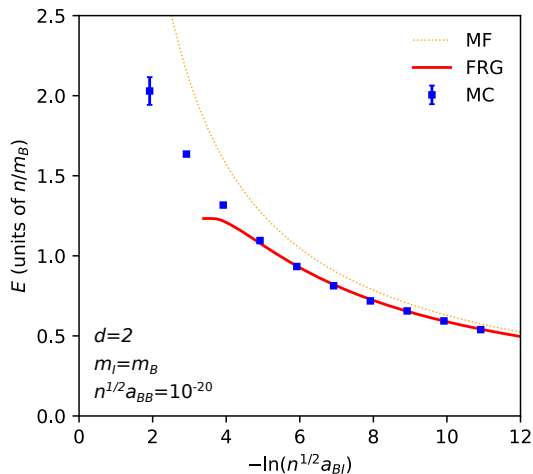
FIG. 2. Polaron energy E of the repulsive branch in two dimensions as a function of $-\log(n^{1/2}a_{BI})$. The solid red line corresponds to FRG calculations. The thin dotted orange line corresponds to the MF solution (17). The blue squares are MC simulations from Ref. [48]. In all cases, $m_B = m_I$ and $n^{1/2}a_{BB} = 10^{-20}$.

achieved experimentally in two-dimensional traps with ^{87}Rb atoms [83, 84]. We compare with MC simulations from Ref. [48], and with the MF solution [48]

$$E = \frac{\pi n/m_R}{|\ln(n^{1/2}a_{BI})|} \,. \tag{17}$$

As in three dimensions, we obtain an excellent agreement with MC simulations for $-\ln(n^{1/2}a_{BI}) \gtrsim 4$. Furthermore, the FRG results show an important improvement over the perturbative solution. This is expected, as the FRG has proved to give a good description of two-dimensional gases [75, 85]. In contrast, perturbative results are less reliable in two dimensions because of the enhanced effect of fluctuations. For stronger interactions ($-\ln(n^{1/2}a_{BI}) \lesssim 4$) the FRG calculations become unreliable due to the breakdown of the initial conditions.

We have checked that we obtain similarly good descriptions of the polaron energy also for other choices of gas parameters and masses $m_B \approx m_I$ in both two and three dimensions. We also provide an estimate of the effective mass in App. C.

IV. ATTRACTIVE BRANCH

We switch now to the description of the quasiparticle excitation which is present at negative energies, the so-called attractive polaron.

Because we now deal with attractive interactions, we have to consider the formation of bound states. In particular, the Bose polaron shows a polaron-to-molecule crossover [25]. Two-body bound states appear as poles in the four-point vertices $\boldsymbol{\Gamma}^{(4)}$. However, in a straightforward application of the DE [see Eq. (4)], all the terms
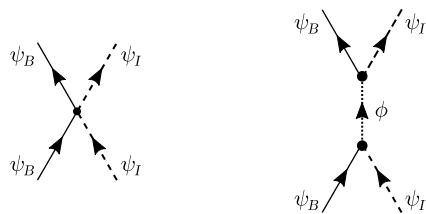

FIG. 3. Tree-level diagram for the scattering between a boson and an impurity before (left) and after (right) the introduction of the auxiliary dimer fields. Solid, dashed, and dotted lines denote bosons, impurities, and dimers, respectively.

in the expansion are regular, and thus they do not account for bound states [55]. We can circumvent this by introducing dimer fields $\phi \sim \psi_B \psi_I$ to mediate the boson-impurity interaction via a Hubbard-Stratonovich transformation [69]. Analogous transformations are used in FRG studies of Fermi gases [61, 62] and few atoms [55]. In the context of Feshbach resonances, the fields ψ_B and ψ_I represent atoms in the open channel, whereas the field ϕ represents dimers in the closed channel [61]. The resulting action takes the form a two-channel model [25]

$$\mathcal{S}[\boldsymbol{\varphi}] = \int_x \left[\psi_B^\dagger \left(\partial_\tau - \frac{\nabla^2}{2m_B} - \mu_B \right) \psi_B \right.$$
$$+ \psi_I^\dagger \left(\partial_\tau - \frac{\nabla^2}{2m_I} - \mu_I \right) \psi_I$$
$$+ \phi^\dagger \left(\partial_\tau - \frac{\nabla^2}{2m_\phi} + \nu_\phi \right) \phi + \frac{g_{BB}}{2}(\psi_B^\dagger \psi_B)^2$$
$$\left. + h \left(\phi^\dagger \psi_B \psi_I + \phi \psi_B^\dagger \psi_I^\dagger \right) \right], \tag{18}$$

where $m_\phi = m_B + m_I$ is the mass of a closed-channel dimer, ν_ϕ is the dimer detuning, and h is the *Feshbach coupling*. The Hubbard-Stratonovich transformation is illustrated in Fig. 3.

We work in the *broad resonance limit* where $h, \nu_\phi \to \infty$, but h^2/ν_ϕ is kept constant [61]. In this limit, by integrating out the dimer fields in Eq. (18) we recover the original one-channel model Eq. (1), and thus both equations are equivalent. Therefore, we stress that in this work Eq. (18) physically describes a one-channel model where ϕ simply acts as an auxiliary field.

Based on action (18), we propose the following ansatz for the effective action in the attractive branch

$$\Gamma_k[\boldsymbol{\phi}] = \int_x \left[\psi_B^\dagger \left(S_B \partial_\tau - \frac{Z_B}{2m_B} \nabla^2 - V_B \partial_\tau^2 \right) \psi_B \right.$$
$$+ \psi_I^\dagger \left(S_I \partial_\tau - \frac{Z_I}{2m_I} \nabla^2 + U_I(\rho_B) \right) \psi_I$$
$$+ \phi^\dagger \left(S_\phi \partial_\tau - \frac{Z_\phi}{2m_\phi} \nabla^2 + U_\phi(\rho_B) \right) \phi$$
$$\left. + H_\phi(\rho_B) \left(\phi^\dagger \psi_B \psi_I + \phi \psi_B^\dagger \psi_I^\dagger \right) + U_B(\rho_B) \right], \tag{19}$$
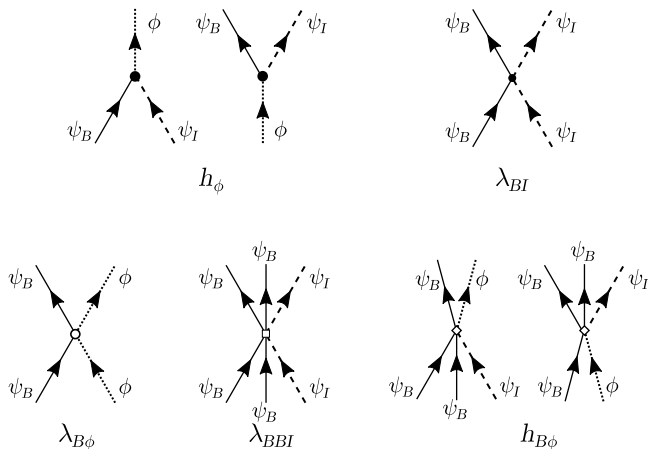
FIG. 4. Two- (upper row) and three-body (bottom row) vertices associated to the interaction between the bosons and the impurity. Solid lines represent the bosons, dashed lines the impurity, and the dotted line the dimer field.

where $\rho_B = \psi_B^\dagger \psi_B$. Our ansatz is similar to those used for the Fermi polaron [69, 71], and, as the repulsive branch, is only valid in two and three dimensions. Note that the dimer fields become dynamical, with flowing renormalization factors S_ϕ and Z_ϕ. We expand the boson effective potential as

$$U_B = -P + \frac{\lambda_{BB}}{2}(\rho_B - \rho_0)^2 \,, \qquad (20)$$

analogously to Eq. (5). As in the repulsive branch, ρ_0 and $\rho_s = Z_B \rho_0$ at $k = 0$ correspond to the physical condensate and superfluid densities of the bosonic medium, respectively. The rest of the functions contain the interactions between the bosonic medium and the impurity. Because three-body correlations are important in the attractive branch, we expand these up to three-body couplings

$$U_I = u_I + \lambda_{BI}(\rho - \rho_0) + \frac{\lambda_{BBI}}{2}(\rho - \rho_0)^2 \,, \qquad (21)$$

$$U_\phi = u_\phi + \lambda_{B\phi}(\rho - \rho_0) \,, \qquad (22)$$

$$H_\phi = h_\phi + h_{B\phi}(\rho - \rho_0) \,. \qquad (23)$$

Here, h_ϕ and λ_{BI} correspond to two-body boson-impurity vertices, whereas $\lambda_{B\phi}$, λ_{BBI} and $h_{B\phi}$ to three-body vertices. These vertices are illustrated in Fig. 4.

The FRG framework enables us to include the effect of three-body correlations by allowing the three-body couplings to flow. In the following, we will want to test the relevance of three-body effects. To switch those off, it is enough to fix the corresponding couplings at zero for all k.

Similarly to the repulsive branch, all the renormalization factors (Z_a, S_a, V_B) and the couplings in U_B, U_I, U_ϕ and H_ϕ, as well as ρ_0, flow with k. We also employ the optimized regulator (6) for all the fields $a = B, I, \phi$. We

provide the flow equations in App. B, and we examine the initial conditions here below.

A. Initial conditions of the RG flow

Similarly to the repulsive branch, the RG flow is started at a high scale $k = \Lambda$ much larger than the healing scale of the bath $k_h = (2m_B \mu_B)^{1/2}$. By imposing that $\Gamma_\Lambda = \mathcal{S}$, we obtain

$$S_B(\Lambda) = Z_B(\Lambda) = S_I(\Lambda) = Z_I(\Lambda) = 1$$

$$V_B(\Lambda) = 0 \,, \quad \rho_0(\Lambda) = \frac{\mu_B}{\lambda_{BB}(\Lambda)} \,, \quad u_I = -\mu_I \,, \quad (24)$$

where $\mu_B > 0$ and $\mu_I < 0$. Note that, in contrast to the repulsive branch, the impurity energy μ_I is negative by construction.

The couplings λ_{BB}, u_ϕ, Z_ϕ and S_ϕ are renormalized in vacuum so they can be connected to physical scattering [62, 74]. The initial condition for λ_{BB} is given by Eq. (8). For the boson-impurity interaction, we consider the boson-impurity scattering length a_{BI} and effective range r_0 as physical inputs. The effective range is necessary to have a well defined three-body sector with attractive interactions in three dimensions. Otherwise, the UV is not well defined since the infinite tower of Efimov trimers which appears in this case lacks a reference scale [34]. At low collision energies, the boson-impurity T matrix takes the form [86, 87]

$$T_{BI} = \begin{cases} \dfrac{2\pi/m_r}{\ln(-4/p_R^2 a_{BI}^2) - 2\gamma_E - \frac{\pi r_0^2}{4}p_R^2 + i\pi} & : d = 2 \\[12pt] \dfrac{2\pi/m_r}{a_{BI}^{-1} - \frac{r_0}{2}p_R^2 + ip_R} & : d = 3 \end{cases} \,, \qquad (25)$$

where

$$p_R = -\sqrt{2m_r \left(p_0 - \frac{\mathbf{p}^2}{2m_\phi} + \mu_\phi\right)} \,, \qquad (26)$$

is the relative momentum, with $\mu_\phi = \mu_B + \mu_I$ and $p_0 = i\omega_p$. At the physical limit $k = 0$ in vacuum, we impose that (see Ref. [88] for details)

$$\left.\frac{h_\phi^2}{\Pi_\phi(p_0, \mathbf{p})}\right|_{k=0} = -T_{BI} \,, \qquad (27)$$

where Π_ϕ is the full dimer self energy. Π_ϕ is related to the couplings in ansatz (19) through $u_\phi = \Pi_\phi(0, \mathbf{0})$, and

$$Z_\phi = 2m_\phi \left.\frac{\partial}{\partial \mathbf{p}^2}\Pi_\phi\right|_{p_0=0, \mathbf{p}=\mathbf{0}} \,, \qquad (28)$$

$$S_\phi = -\left.\frac{\partial}{\partial p_0}\Pi_\phi\right|_{p_0=0, \mathbf{p}=\mathbf{0}} \,. \qquad (29)$$

We obtain the following initial conditions [88]

$$\left.\frac{u_\phi}{h_\phi^2}\right|_\Lambda = \begin{cases} \dfrac{m_r}{2\pi}\left(\ln(a_{BI}^2\Lambda^2/4) + 2\gamma_E - 1\right) & : d = 2 \\[12pt] \dfrac{2m_r}{3\pi^2}\Lambda - \dfrac{m_r}{2\pi a_{BB}} & : d = 3 \end{cases} \,, \qquad (30)$$

and

$$\frac{Z_\phi}{h_\phi^2}\bigg|_\Lambda = \frac{S_\phi}{h_\phi^2}\bigg|_\Lambda = \begin{cases} \frac{m_r^2}{\pi}\left(\frac{2}{\Lambda^2} - \frac{\pi}{4}r_0^2\right) & : d = 2 \\ \frac{m_r^2}{\pi^2}\left(\frac{8}{3\Lambda} - \frac{\pi}{2}r_0\right) & : d = 3 \end{cases}. \quad (31)$$

Note that u_ϕ and h_ϕ are chosen freely as long as they satisfy Eq. (30).

Since we work in the broad resonance limit, we have naturally $r_0 > 0$ [89, 90]. In three dimensions, a positive effective range ensures that the dimer fields become non-dynamical in the UV with $Z_\phi, S_\phi \to 0$, and so our ansatz describes a one-channel model. For details on the FRG for narrow resonances, see Ref. [61].

The scattering length a_{BB} sets a lower bound for the range of the boson-boson interaction, whereas r_0 sets the range of the attractive boson-impurity interaction. Analogously to the repulsive branch, we must restrict the flow to momenta smaller than a_{BB}^{-1} and r_0^{-1} in order for our approximation of contact potentials to be valid. Therefore, the initial scale has to satisfy $\Lambda < \min(a_{BB}^{-1}, r_0^{-1})$. We stress again that because of the renormalizations (30) and (31), the results are independent of the choice of Λ as long as $\Lambda \gg k_h$.

In contrast to purely repulsive potentials, for attractive potentials the scattering length can be tuned independently of the range. Therefore, in the attractive branch we can choose a_{BI} freely. This enables us to study the regime of strong boson-impurity coupling, including the unitary limit $a_{BI} \to \infty$ in three dimensions [62]. In contrast, in the repulsive branch the initial scale Λ is heavily restricted by a_{BI} [see discussion after Eq. (8)].

The couplings not mentioned so far are not present in the microscopic theory (18), and so their values at $k = \Lambda$ are zero. In particular, the three-body couplings are zero in the UV, and they are only generated as k is lowered. To capture the effect of three-body correlations at high scales, we must start the RG flow at a high scale nearby the range of the interactions: $\Lambda \approx \min(a_{BB}^{-1}, r_0^{-1})$.

B. Propagator and polaron energy

In the attractive branch, the inverse propagator for ansatz (19) reads

$$\mathbf{G}_k^{-1}(q) = \begin{pmatrix} \mathbf{G}_{k,B}^{-1}(q) & \mathbf{0} \\ \mathbf{0} & \mathbf{G}_{k,I\phi}^{-1}(q) \end{pmatrix}, \quad (32)$$

where $G_{k,B}^{-1}$ is given in Eq. (10), and

$$\mathbf{G}_{k,I\phi}^{-1}(q) = \begin{pmatrix} E_{I,k}(\mathbf{q};\rho_B) + iS_I\omega & 0 & \rho_B^{1/2}H_\phi(\rho_B) & 0 \\ 0 & E_{I,k}(\mathbf{q};\rho_B) - iS_I\omega & 0 & \rho_B^{1/2}H_\phi(\rho_B) \\ \rho_B^{1/2}H_\phi(\rho_B) & 0 & E_{\phi,k}(\mathbf{q};\rho_B) + iS_\phi\omega & 0 \\ 0 & \rho_B^{1/2}H_\phi(\rho_B) & 0 & E_{\phi,k}(\mathbf{q};\rho_B) - iS_\phi\omega \end{pmatrix}, \quad (33)$$

is the impurity-dimer inverse propagator, with

$$E_{I,k}(\mathbf{q};\rho_B) = Z_I\frac{\mathbf{q}^2}{2m_I} + U_I(\rho_B) + R_{k,I}(\mathbf{q}), \quad (34)$$

$$E_{\phi,k}(\mathbf{q};\rho_B) = Z_\phi\frac{\mathbf{q}^2}{2m_\phi} + U_\phi(\rho_B) + R_{k,\phi}(\mathbf{q}). \quad (35)$$

In contrast to the problem of an impurity in a Fermi bath, whose ground state features a sharp transition between a polaron and a dressed dimer, the Bose polaron prob-

lem shows a smooth polaron-to-molecule crossover. We can understand this from Eq. (33), where if $\rho_0 > 0$ we can not separate $\mathbf{G}_{k,I\phi}^{-1}$ into independent impurity and dimer propagators. Therefore, the impurity and dimer propagators are hybridized, and we can not identify a polaron or a molecule phase (for more details, we refer to Ref. [25]).

To find the ground state energy μ_I, we search for the pole of the Green's function $\mathbf{G}_{I\phi}$, as we did for the repulsive branch in Sec. III B. By taking $\det(\mathbf{G}_{k,I\phi}^{-1}) = 0$ at the minimum $\rho_B = \rho_0$, we find two poles

$$q_{0,\pm}^*(\mathbf{q}) = \frac{1}{2}\left[\frac{E_{I,k}(\mathbf{q})}{S_I} + \frac{E_{\phi,k}(\mathbf{q})}{S_\phi} \pm \sqrt{\left(\frac{E_{I,k}(\mathbf{q})}{S_I} + \frac{E_{\phi,k}(\mathbf{q})}{S_\phi}\right)^2 - \frac{4}{S_IS_\phi}(E_{I,k}(\mathbf{q})E_{\phi,k}(\mathbf{q}) - h_\phi^2\rho_0)}\right], \quad (36)$$

where E_I and E_ϕ are defined in Eqs. (34) and (35). As with the repulsive branch, we identify the choice of μ_I

that gives $q_{0,\pm}^*(\mathbf{0}) = 0$ for $k \to 0$ as the energy of the polaron. Similarly, choices of μ_I that do not fulfill this

condition are not physical.

We find that $q_{0,+}^*(\mathbf{0})$ and $q_{0,-}^*(\mathbf{0})$ go to zero at the same impurity energy μ_I, and thus there is one ground state energy for each combination of interaction strengths. This can change at finite temperatures, where the spectrum can split into more than one quasiparticle [29, 91]. We provide details of the flows in App. B.

C. Results

In the following, we evaluate the polaron energy in both two and three dimensions, and we compare it with available analytical and experimental results. To quantify the effect of three-body correlations, we present curves which include only two-body correlations (2B) and both two- and three-body correlations (2B+3B).

1. Three dimensions

The attractive branch of the three-dimensional polaron at zero temperature has been previously investigated in various works. To test the robustness of our FRG calculations, we compare with MC simulations, solutions of the Gross-Pitaevskii equation (GPe), ladder calculations and experimental data.

Fig. 5 shows the polaron energy for three choices of masses and gas parameters. The panels (a), (b) and (c) simulate, respectively, the conditions of the Aarhus [19], JILA [20], and MIT [21] experiments. We present calculations with only two-body interactions and $r_0 = 0$ (because for the interactions we investigated the two-body sector is only weakly sensitive to r_0), and with two- and three-body interactions with both $r_0 = 0$ and $r_0 > 0$. We use the effective ranges r_0 computed in Ref. [37].

In panels (a) and (b) we compare with experimental data, GPe calculations [37], and MC simulations [47]. In addition, we compare with the perturbative solution (16), where $I(2.2) \approx 1.78$ and $I(1/1.72) \approx 1.99$. Additionally, in panel (a) we compare with ladder calculations from Ref. [26], which give an upper bound for the energy. We observe a noticeable effect of three-body correlations in panels (a) and (b), as well of the effective range. In contrast, in panel (c) three-body effects are not as important. This is in agreement with previous studies that showed that three-body effects are more important for lighter impurities and at lower bath densities [34, 92].

In the weakly interacting regime $(n^{1/3}a_{BI})^{-1} \lesssim -4$, our FRG calculations recover the expected result from perturbation theory (16). For stronger interactions, $(n^{1/3}a_{BI})^{-1} \gtrsim -4$, our FRG is in very good agreeement with both MC and GPe results. We obtain the best agreement with MC by including three-body correlations with $r_0 = 0$. Nevertheless, also our calculations with finite effective range are in reasonable agreement with experiment.
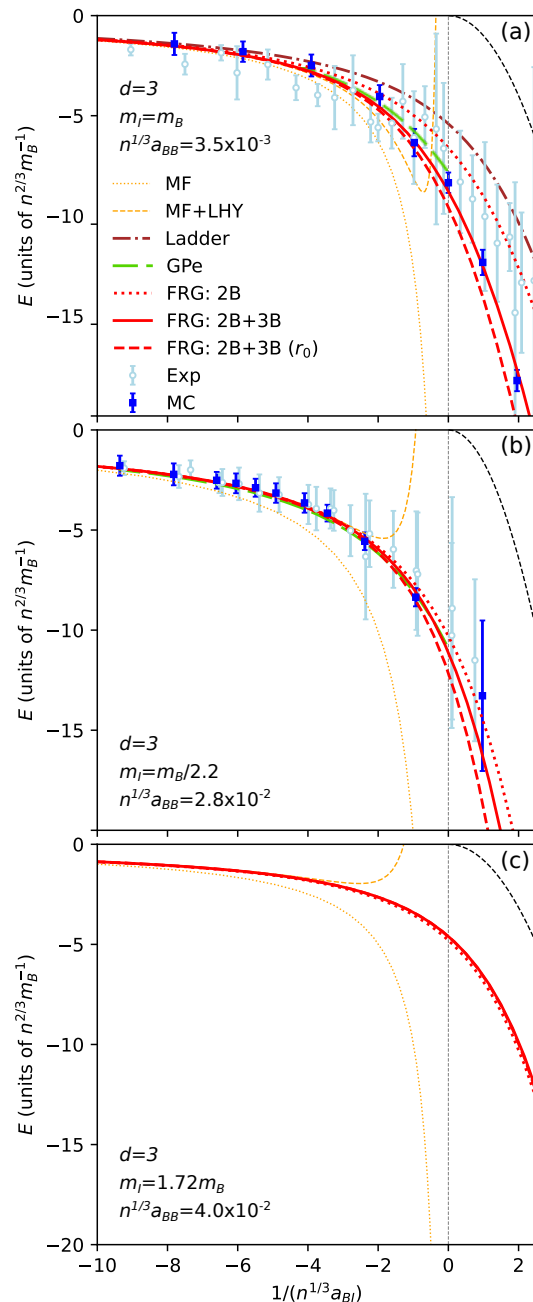

FIG. 5. Polaron energy in three dimensions as a function of $(n^{1/3}a_{BI})^{-1}$. The red lines correspond to FRG calculations with only 2B interactions (dotted), 2B+3B interactions with $r_0 = 0$ (solid), and 2B+3B interactions with $r_0 = 3, 1.5, 0.6a_{BB}$ (dashed) for (a), (b), and (c), respectively. The thin orange lines show the perturbative solution (16) at the MF level (dotted), and with the first correction (dashed). The green dashed lines are GPe calculations from Ref. [37] [in panel (b) the green line is underneath the solid red line]. The dash-dotted brown line shows ladder calculations from Ref. [26], the blue squares are MC simulations from Ref. [47], and the light blue circles are experimental data from Refs. [19, 47] (a) and [20] (b). The dashed black lines show the binding energy in vacuum $\epsilon_b = -(2m_R a_{BI}^2)^{-1}\Theta(a_{BI})$.
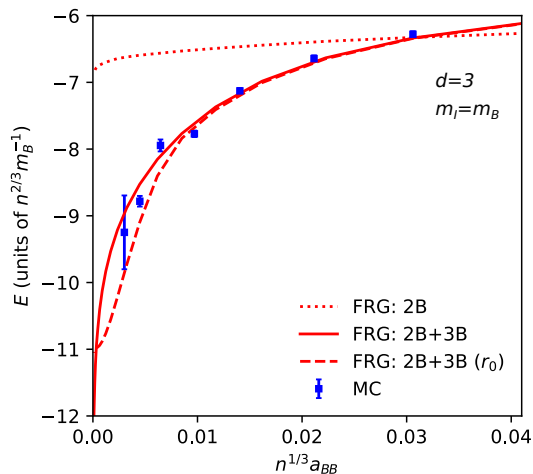
FIG. 6. Polaron energy in three dimensions at unitarity $a_{BI} \to \infty$ for $m_B = m_I$ as a function of the gas parameter $n^{1/3}a_{BB}$. The red lines correspond to FRG calculations with only 2B interactions (dotted), 2B+3B interactions with $r_0 = 0$ (solid), and 2B+3B interaction with $r_0 = 2.2 \times 10^{-3}/(m_B\mu_B)^{1/2} > 0$. The blue circles are MC simulations from Ref. [45].

To examine the effect of the gas parameter, in Fig. 6 we show the polaron energy as a function of $n^{1/3}a_{BB}$ at unitarity, where three-body correlations are important. We find that the effect of three-body correlations depends strongly on the gas parameter, in agreement with previous studies [34]. As we approach the vacuum limit $n^{1/3}a_{BB} \to 0$, three-body correlations become much more important, significantly decreasing the polaron energy. In particular, we obtain a good agreement with MC simulations from Ref. [45] by considering three-body effects. This confirms both the importance of three-body physics and also the robustness of our calculations.

At low gas parameters, the polaron energy is more sensitive to the effective range. In particular, with three-body interactions, the polaron energy goes to a finite value with a finite effective range, whereas we are not able to find a bound with $r_0 = 0$. As explained in detail in Ref. [34], with $r_0 = 0$ there are infinite Efimov trimers in vacuum, and so the energy diverges at the vacuum limit. In contrast, for $r_0 > 0$ there is a well defined deepest Efimov state, and therefore the energy saturates to a finite value. Finally, let us mention that the limit of very low gas parameters is extremely delicate [34, 37, 38, 40]. Indeed, in the limit $a_{BB} \to 0$ the bath becomes infinitely compressible, and thus multi-body correlations play an increasing importance. To study such regime with FRG, one would need to include further higher order couplings in the ansatz.

2. Two dimensions

The two-dimensional Bose polaron has been studied in detail only recently, with MC simulations in Ref. [48]. Here, we provide results for various conditions achieved in current experiments [83, 84].

Fig. 7 shows results for three different combination of masses and the gas parameter $n^{1/2}a_{BI} = 10^{-20}$. All the calculations use $r_0 = 0$. We find that our calculations are insensitive to reasonably chosen effective ranges. This is not unexpected. In two dimensions, there are no Efimov trimers in vacuum, with only two three-body bound states [93].

In panel (a) we compare with MC simulations from Ref. [48]. Additionally, we compare with the perturbative solution (17). In all cases, we obtain a noticeable effect of three-body correlations. In particular, in panel (a) we obtain a better agreement with the MC simulations by considering three-body effects. However, we do not obtain an agreement as good as in three dimensions. This could either be an effect of the derivative expansion or of not considering higher-order couplings. We stress that because fluctuations are enhanced in low dimensions, it is expected that our approximation is less robust than in three dimensions.

To study the effect of the density of the medium, in Fig. 8 we show the polaron energy in the strong coupling regime as a function of the bath density. We show results for $\ln(n^{1/2}a_{BI}) = 0$, which can not be described by the perturbative solution (17). We explore a wide range of gas parameters. We note that recent experiments have produced two-dimensional bosonic gases with gas parameters as high as $n^{1/2}a_{BB} \approx 10^{-9} - 10^{-4}$ without many losses [94, 95].

As in three dimensions, we observe an important effect of three-body correlations. However, the energy seems to converge to a finite value for the vacuum gas limit with and without three-body effects, even with zero effective range. This is expected. As mentioned, in two dimensions there are only two well defined tree-body bound states in vacuum [93] instead of infinite Efimov trimers. Nevertheless, we do not reach the value of the binding energy of the deepest trimer in vacuum $E \approx 16.5\epsilon_b$, where $\epsilon_b = -2/(m_r e^{2\gamma_E}a_{BI}^2)$. In Fig. 8, this corresponds to $Em_B/n \approx -21$. This is probably due to our truncation of the derivative expansion, which does not describe few-body physics accurately [55]. We expect that the inclusion of further couplings will improve the convergence.

V. CONCLUSIONS

In this work, we studied the Bose polaron at zero temperature in two and three dimensions with the FRG. We approximated the effective action by means of a derivative expansion, which enabled us to find the ground state energies of the polaron by following the flow of the scale-dependent poles of the impurity's propagator.
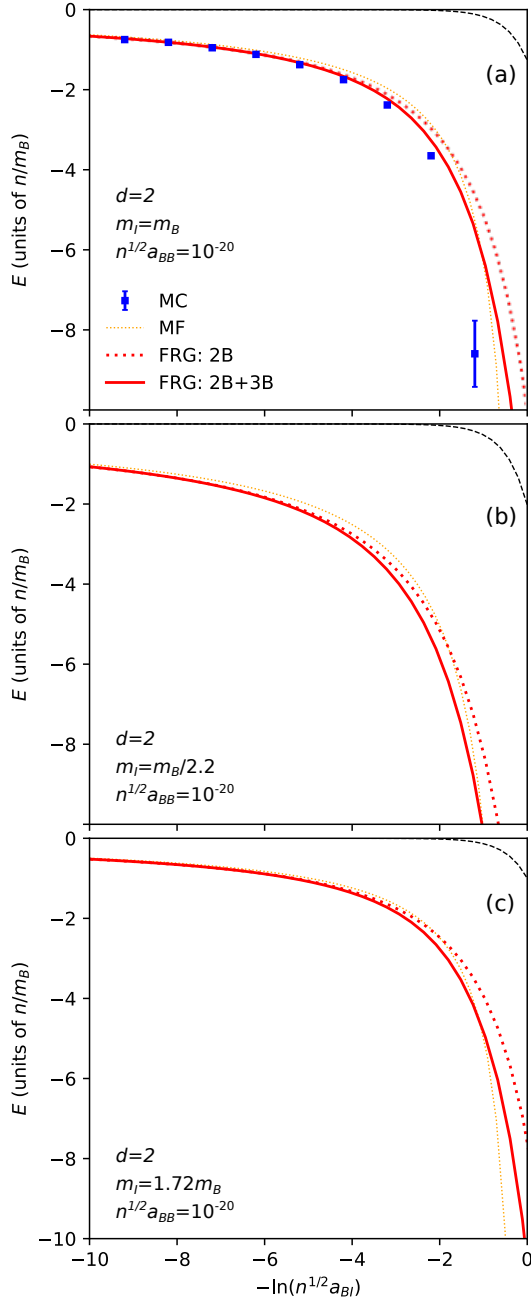
FIG. 7. Polaron energy in two dimensions as a function of $-\log(n^{1/2}a_{BI})$. Masses and gas parameters are given within the figures. The red lines correspond to FRG calculations with only 2B interactions (dotted), and 2B+3B interactions with $r_0 = 0$ (solid). The thin orange gray lines show the MF solution (17). The blue squares are MC simulations from Ref. [48]. The dashed black lines are the boson-impurity binding energy $\epsilon_b = -2/(m_r e^{2\gamma_E} a_{BI}^2)$.
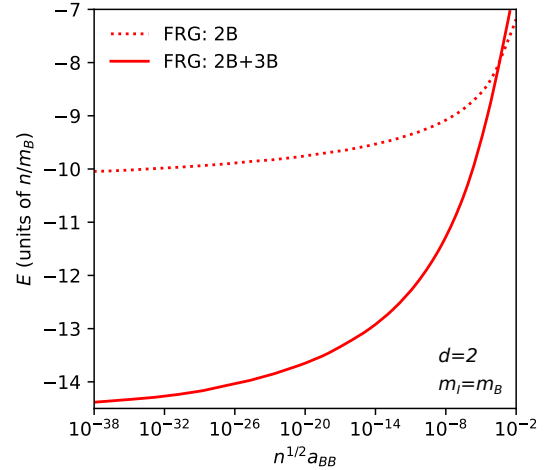
FIG. 8. Polaron energy in two dimensions at $\ln(n^{1/2}a_{BI}) = 0$ for $m_B = m_I$ as a function of the gas parameter $n^{1/2}a_{BB}$. The red lines show FRG calculations with 2B interactions only (dotted), and 2B+3B interactions with $r_0 = 0$ (solid).

In addition, in the attractive branch, we added the effect of three-body correlations by considering up to three-body couplings in the derivative expansion.

We obtained polaron energies in good agreement with state-of-the-art theoretical and experimental results. In particular, in the attractive branch, we obtained the best agreement by adding three-body effects. Overall, we showed that the FRG can successfully describe the regime of strong coupling in both two and three dimensions.

Throughout this manuscript, we focused on cases where $0.5 \lesssim m_I/m_B \lesssim 2$. The reason is twofold. On one side, for heavy impurities, homogeneous fields might not provide a good description of static particles. On the other side, for light impurities, the attractive branch is strongly influenced by Efimov trimers [92], which require a careful treatment, beyond the scope of the current work.

Having demonstrated that the Bose polaron can be successfully described with the FRG, there are several extensions of this work that we plan to explore in the future. First, we intend to consider the full momentum dependence of the flowing couplings by employing a vertex expansion [51] in order to give a more robust description of the Bose polaron. This will enable us to obtain the full Green's function, which is not accessible within the derivative expansion, and to study dynamical properties, as well as decay rates. Furthermore, the account of momentum dependent vertices is necessary to accurately capture few-body physics, including the onset of Efimov states, which are beautifully captured with the FRG as periodic cycles in the RG flow [55]. We also plan to explore the effect of four- and more-body correlations by adding higher-order couplings.

On top of the current works on Bose and Fermi polarons, the FRG could be used to study impurities in other scenarios. A small finite number of impurities is

We studied both the repulsive and attractive branches of the Bose polaron. In the attractive branch, we introduced dimer fields via a Hubbard-Stratonovich transformation to mediate the boson-impurity interaction. This enabled us to access the regime of strong coupling easily.

a natural extension of this work, and systems with a small population of impurities can be studied as quantum mixtures with large population imbalances [67, 71]. Furthermore, polarons in optical lattices could be naturally studied by employing the lattice implementation of the FRG [96], which has proved very successful in describing strongly-correlated lattice gases [97]. Using impurities to probe topological excitations is, presently, a topic of great interest [98–100], and the FRG may be a good tool to address them at strong coupling. Finally, polarons at finite temperatures can be easily studied by using the Matsubara formalism. Particularly interesting would be to examine the impact of the BKT transition on the properties of two-dimensional Bose polarons.

Appendix A: RG flow of the repulsive branch

1. Flow equations

In the DE all the couplings are momentum-independent $f(q) = f$, and their flows are simply obtained by differentiating the Wetterich equation (2). Because there is no feedback of the impurity onto the medium, the flow equations for the bosonic couplings (ρ_0, λ_{BB}, Z_B, S_B and V_B) are identical to those of a one-component Bose gas. Thus, we refer to Ref. [74] for details. Also, note that it is not necessary to follow the flow of the k-dependent pressure P, as it does not affect the flow of the rest of the couplings.

The flows of the couplings associated to the impurity

are dictated by

$$\partial_k u_I = \partial_k \Gamma^{(2)}_{k,I^\dagger I}\Big|_{\rho_0,p=0}, \tag{A1}$$

$$\partial_k \lambda_{BI} = \frac{\partial}{\partial \rho_B}(\partial_k \Gamma^{(2)}_{k,I^\dagger I})\Big|_{\rho_0,p=0}, \tag{A2}$$

$$\partial_k Z_I = 2m_I \frac{\partial}{\partial \mathbf{p}^2}(\partial_k \Gamma^{(2)}_{k,I^\dagger I})\Big|_{\rho_0,p=0}, \tag{A3}$$

$$\partial_k S_I = i\frac{\partial}{\partial \omega_p}(\partial_k \Gamma^{(2)}_{k,I^\dagger I})\Big|_{\rho_0,p=0}, \tag{A4}$$

where $\partial_k \Gamma_k$ is obtained from the Wetterich equation (2), $p = (\omega_p, \mathbf{p})$ is an external momentum which is taken to zero after differentiating, and the two-point function is defined as

$$\Gamma^{(2)}_{k,I^\dagger I} = \frac{\delta^2 \Gamma}{\delta \psi_I^\dagger \delta \psi_I}. \tag{A5}$$

We note that we take $p = 0$ because in a DE all the couplings are momentum-independent, and thus we follow the flow at zero momentum [52]. Studies at finite momenta can be implemented within a vertex expansion, where the ansatz for Γ is proposed in terms of momentum-dependent vertices instead of simple derivatives [51]. However, to solve the RG flow in a vertex expansion, we usually need to perform sophisticated calculations, such as with the BMW approximation [79], which are beyond the scope of this work.

Because we follow the flow at the minimum ρ_0, we evaluate at $\rho_B = \rho_0$ after taking the derivatives. The diagrams that contribute to the flow of $\Gamma^{(2)}_{k,I^\dagger I}$ are shown in Fig. 9. They give the following expression

$$\partial_k \Gamma^{(2)}_{k,I^\dagger I} = \tilde{\partial}_k \int_q \left[4\rho_B \lambda_{BI}^2 \frac{(E_{2,k}(\mathbf{q}) + V_B\omega^2)E_{I,k}(\mathbf{q}+\mathbf{p})}{\det_B(q)\det_I(q+p)} \right.$$
$$\left. - \frac{\lambda_{BI}(E_{1,k}(\mathbf{q}) + E_{2,k}(\mathbf{q}) + 2V_B\omega^2)}{2\det_B(q)} \right], \tag{A6}$$

where $\tilde{\partial}_k$ is a k-derivative that only acts on the regulators, E_1, E_2 and E_I are given in Eqs. (11,12) and (14), and

$$\det_B(q) = S_B^2\omega^2 + (E_{1,k}(\mathbf{q}) + V_B\omega^2)(E_{2,k}(\mathbf{q}) + V_B\omega^2), \tag{A7}$$

$$\det_I(q) = S_I^2\omega^2 + E_{I,k}(\mathbf{q})^2. \tag{A8}$$

Note that E_1, E_2 and E_I still depend on ρ_B, which is only taken to $\rho_B = \rho_0$ after taking all the derivatives. Finally, the integral over internal momentum $q = (\omega, \mathbf{q})$ is defined as

$$\int_q = \int_{-\infty}^{\infty} \frac{d\omega}{2\pi} \int \frac{d^d\mathbf{q}}{(2\pi)^d}. \tag{A9}$$

2. Examples of flows

Fig. (10) shows the flow of u_I for different μ_I for chosen parameters for the bosonic medium and the boson-
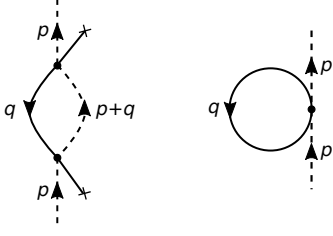
FIG. 9. Diagrams that contribute to the flow of $\Gamma^{(2)}_{k,I^\dagger I}$. Solid and dashed lines denote bosons and impurities, respectively. The cross denotes a boson field evaluated at its background value $\langle \psi_B \rangle = \sqrt{\rho_B}$.
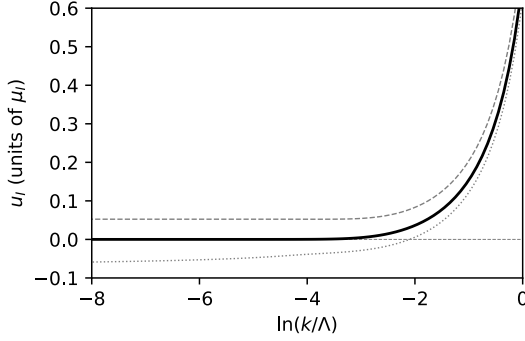

FIG. 10. Flow of u_I in three dimensions in the repulsive branch for $n^{1/3}a_{BB} = 3.5 \times 10^{-3}$ at $(n^{1/3}a_{BI})^{-1} = 10$. The solid line corresponds to the flow obtained for the ground state energy μ_I^*, the thin dashed line to a flow obtained with $\mu_I < \mu_I^*$, and the thin dotted to a flow obtained with $\mu_I > \mu_I^*$.

impurity scattering length. At the physical polaron energy μ_I^*, the couplings u_I flows to zero (solid black line), giving a vanishing $q_0^*(\mathbf{0})$. In contrast, for $\mu_I < \mu_I^*$ the coupling u_I saturates to finite values greater than zero, whereas for $\mu_I < \mu_I^*$ it goes to negative values. Thus, values of $\mu_I \neq \mu_I^*$ do not correspond to physical energies of the impurity.

This behavior is found for any combinations of parameters in both two and three dimensions.

Appendix B: RG flow of the attractive branch

1. Flow equations and k-dependent dimer fields

The strategy is similar to that used for the repulsive branch in App. A, where the flow of the momentum-independent couplings is obtained by differentiating the Wetterich equation. The flow of the bosonic couplings (ρ_0, λ_{BB}, Z_B, S_B and V_B) is given by those of a one-component Bose gas [74], whereas the flow of the couplings in Eqs. (21-23) can be extracted from the flow of
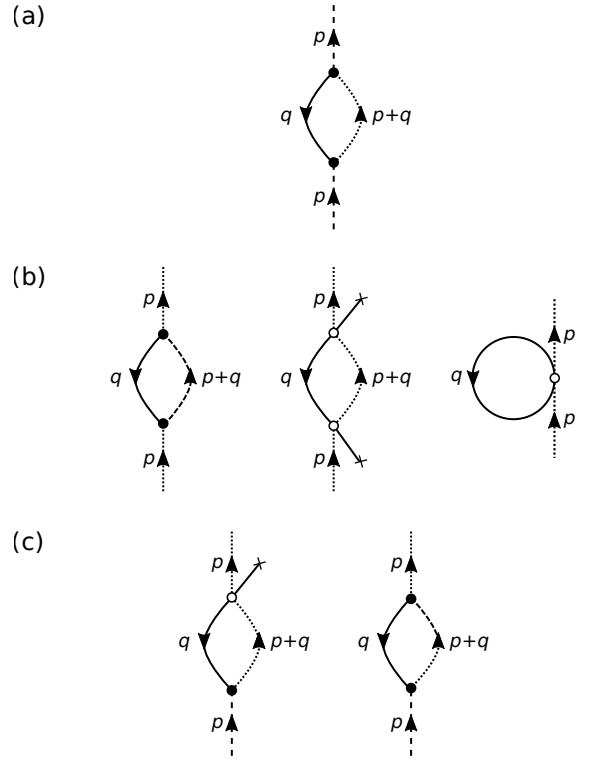

FIG. 11. Diagrams that contribute to the flow of $\Gamma^{(2)}_{k,I^\dagger I}$ (a), $\Gamma^{(2)}_{k,\phi^\dagger \phi}$ (b), and $\Gamma^{(2)}_{k,\phi^\dagger I}$ (c). Solid, dashed and dotted lines denote bosons, impurities and dimers, respectively. The crosses denotes boson fields evaluated at their background value $\langle \psi_B \rangle = \sqrt{\rho_B}$.

the two point functions

$$\partial_k U_I = \partial_k \Gamma^{(2)}_{I^\dagger I}\Big|_{p=0}, \tag{B1}$$

$$\partial_k U_\phi = \partial_k \Gamma^{(2)}_{\phi^\dagger \phi}\Big|_{p=0}, \tag{B2}$$

$$\partial_k H_\phi = \partial_k \Gamma^{(2)}_{I^\dagger \phi}\Big|_{p=0}, \tag{B3}$$

where the derivatives in $\Gamma^{(2)}$ are defined in the same way as in Eq. (A5). We provide their explicit expression in the next subsection. The specific flow of the different couplings within U_I, U_ϕ, and H_ϕ are obtained by taking ρ_B derivatives and then evaluating at $\rho_B = \rho_0$. Also, as with the repulsive branch, we follow the flow at zero momentum, and thus we evaluate at $p = 0$.

To simplify the flow equations, we introduce k-dependent dimer fields ϕ_k to eliminate the flow of some of the couplings. If we introduce k-dependent fields, the Wetterich equation becomes [51]

$$\partial_k \Gamma_k = \frac{1}{2} \, \text{tr} \left[(\mathbf{\Gamma}^{(2)}_k + \mathbf{R}_k)^{-1} \partial_k \mathbf{R}_k \right] + \frac{\delta \Gamma_k}{\delta \boldsymbol{\phi}} \cdot \partial_k \boldsymbol{\phi}_k. \tag{B4}$$

We choose the k-dependent fields so that these eliminate the flow of the couplings λ_{BI}, λ_{BBI} and $h_{B\phi}$. Similar eliminations have been used in FRG studies of few

bosons [56–58] and Fermi gases [63]. This elimination means that these couplings will not flow with k and will remain at zero during the entire flow. We use k-dependent dimer fields defined as

$$\partial_k \phi_k = f_{2B}(k)\psi_B \psi_I + f_{3B}(k)(\rho_B - \rho_0)\psi_B \psi_I + g_{3B}(k)(\rho - \rho_0)\phi_k \,,$$ (B5)

$$\partial_k \phi_k^\dagger = f_{2B}(k)\psi_B^\dagger \psi_I^\dagger + f_{3B}(k)(\rho_B - \rho_0)\psi_B^\dagger \psi_I^\dagger + g_{3B}(k)(\rho - \rho_0)\phi_k^\dagger \,,$$ (B6)

where the functions f_{2B}, f_{3B} and g_{3B} are chosen to eliminate the flows of λ_{BI}, λ_{BBI} and $h_{B\phi}$. Following Eq. (B4), the flow of these couplings is dictated by

$$\partial_k \lambda_{BI} = \partial_k \lambda_{BI}\Big|_\phi + 2f_{2B}h_\phi + 2f_{3B}h_\phi \rho_0 \,,$$ (B7)

$$\partial_k \lambda_{BBI} = \partial_k \lambda_{BBI}\Big|_\phi + 4f_{3B}h_\phi \,,$$ (B8)

$$\partial_k h_{B\phi} = \partial_k h_{B\phi}\Big|_\phi + f_{2B}\lambda_{B\phi} + f_{3B}u_\phi + g_{3B}h_\phi \,,$$ (B9)

where $\partial_k f\big|_\phi$ corresponds to the flow of these couplings when the dimer fields are kept fixed. By imposing that the flow of these couplings remain at zero ($\partial_k f = 0$), we obtain

$$f_{2B} = -\frac{\partial \lambda_{BI}\big|_\phi}{2h_\phi} + \frac{\rho_0}{4h_\phi}\partial_k \lambda_{BBI}\Big|_\phi \,,$$ (B10)

$$f_{3B} = -\frac{\partial_k \lambda_{BBI}\big|_\phi}{4h_\phi} \,,$$ (B11)

$$g_{3B} = -\frac{\partial_k h_{B\phi}\big|_\phi}{h_\phi} + \frac{\lambda_{B\phi}}{2h_\phi^2}\partial_k \lambda_{BI}\Big|_\phi$$
$$- \frac{\lambda_{B\phi}\rho_0 - u_\phi}{4h_\phi^2}\partial_k \lambda_{BBI}\Big|_\phi \,.$$ (B12)

The flow of the rest of the couplings is then dictated by

$$\partial_k u_i = \partial_k u_i\Big|_{\phi,\rho_0} + 2f_{2B}h_\phi \rho_0 \,,$$ (B13)

$$\partial_k u_\phi = \partial_k u_\phi\Big|_{\phi,\rho_0} + \lambda_{B\phi}\partial_k \rho_0 \,,$$ (B14)

$$\partial_k \lambda_{B\phi} = \partial_k \lambda_{B\phi}\Big|_{\phi,\rho_0} + 2g_{3B}u_\phi \,,$$ (B15)

$$\partial_k h_\phi = \partial_k h_\phi\Big|_{\phi,\rho_0} + f_{2B}u_\phi \,,$$ (B16)

where we have evaluated at $\rho_B = \rho_0$. Note that although we eliminate the flow of some couplings, their effect is taken into account by the functions in Eqs. (B10-B12). We stress that now $\lambda_{B\phi}$ carries the entire three-body physics.

Finally, the flow of the renormalization factors is simply given by

$$\partial_k Z_a = 2m_a \frac{\partial}{\partial \mathbf{p}^2}\dot{\Gamma}^{(2)}_{a^\dagger a}\Big|_{p=0,\rho_0} \,,$$ (B17)

$$\partial_k S_a = i\frac{\partial}{\partial \omega_p}\dot{\Gamma}^{(2)}_{a^\dagger a}\Big|_{p=0,\rho_0} \,,$$ (B18)

where $a = I, \phi$, and we evaluate at zero external momentum after taking the momentum derivatives.

2. Expressions for the two-point function

As explained in the previous subsection, to follow the flow of the couplings we need the two-point functions $\Gamma^{(2)}_{I^\dagger I}$, $\Gamma^{(2)}_{\phi^\dagger \phi}$ and $\Gamma^{(2)}_{I^\dagger \phi}$. The diagrams contributing to their flow are shown in Fig. 11. Note that thanks to the elimination of some couplings, only a few diagrams contribute. The explicit expressions are

$$\partial_k \Gamma^{(2)}_{k,I^\dagger I} = \tilde{\partial}_k \int_q \frac{h_\phi^2}{2} \left[\frac{D_{B,+}(q) D_{I,-}(q+p)}{\det_B(q) \det_{I\phi,-}(q+p)} + (+ \leftrightarrow -) \right], \tag{B19}$$

$$\partial_k \Gamma^{(2)}_{k,\phi^\dagger \phi} = \tilde{\partial}_k \int_q \left[\frac{h_\phi^2}{2} \left(\frac{D_{B,-}(q) D_{\phi,-}(q+p)}{\det_B(q) \det_{I\phi,-}(q+p)} + (+ \leftrightarrow -) \right) + \frac{2\rho_B \lambda_{B\phi}^2 C_2(q)}{\det_B(q)} \left(\frac{D_{I,-}(q+p)}{\det_{I\phi,-}(q+p)} + (+ \leftrightarrow -) \right) \right.$$
$$\left. - \frac{\lambda_{B\phi}}{2} \frac{C_1(q) + C_2(q)}{\det_B(q)} \right], \tag{B20}$$

$$\partial_k \Gamma^{(2)}_{k,\phi^\dagger I} = \tilde{\partial}_k \int_{\mathbf{q}} \left[h_\phi \rho_B^{1/2} \lambda_{B\phi} \left(\frac{D_{2,+}(q) D_{I,-}(q+p)}{\det_B(q) \det_{I\phi,-}(q+p)} + (+ \leftrightarrow -) \right) + \frac{h_\phi^3 \rho_B^{1/2}}{2} \frac{\Delta E_B(\mathbf{q})}{\det_B(q)} \left(\frac{1}{\det_{I\phi,-}(q+p)} - (+ \leftrightarrow -) \right) \right], \tag{B21}$$

where $\tilde{\partial}_k$ is a k-derivative that only acts on the regulators, $(+ \leftrightarrow -)$ denotes changing the signs in the subscripts of the previous expression,

$$C_i(q) = E_{k,i}(\mathbf{q}) + V_B \omega^2, \qquad i = 1, 2 \tag{B22}$$

$$D_{2,\pm}(q) = E_{k,2}(\mathbf{q}) + 2V_B \omega^2 \pm 2iS_B \omega, \tag{B23}$$

$$D_{B,\pm}(q) = D_{2,\pm}(q) + E_{k,1}(\mathbf{q}), \tag{B24}$$

$$D_{a,\pm}(q) = E_{k,a}(\mathbf{q}) + iS_a \omega, \qquad a = I, \phi \tag{B25}$$

$$\det_{I\phi,\pm}(q) = D_{I,\pm}(q) D_{\phi,\pm}(q) - \rho_B h_\phi^2, \tag{B26}$$

$$\Delta E_B(\mathbf{q}) = E_{1,k}(\mathbf{q}) - E_{2,k}(\mathbf{q}) \tag{B27}$$

and $\det_B$ is defined in Eq. (A7). The regulated energies $E_{k,1}$ and $E_{k,2}$ are defined in Eqs. (11,12), and $E_{k,I}$ and $E_{k,\phi}$ in Eqs. (34,35). We again stress that the regulated energies depend on ρ_B, which is only evaluated at $\rho_B = \rho_0$ after taking the derivatives.

3. RG flow examples

Here we show some examples of RG flows to illustrate the behavior of the couplings as functions of k. Fig. 12 shows flows of the couplings Z_I, S_I, Z_ϕ, S_ϕ and u_I in three dimensions and unitarity ($a_{BI} \to \infty$) for a chosen gas parameter for the bosonic medium. The black lines are flows at the physical polaron energy μ_I^* which gives $q_{0,\pm}^*(\mathbf{0}) \to 0$ for $k \to 0$ (see Sec. IV B), whereas the thin gray lines correspond to flows obtained with an energy $\mu_I < \mu_I^*$.

The renormalization factors (panels (a) and (b)) diverge at μ_I^*. At this energy μ_I^* the rest of the couplings in Eq. (36) vanish or saturate to finite values. For example, u_I vanishes as k goes to zero (panel (c)). All this results in the vanishing of $q_{0,\pm}^*(\mathbf{0})$ at μ_I^*. On the other hand, for $\mu_I < \mu_I^*$ the renormalization factors sature to finite values, and thus $q_{0,\pm}^*(\mathbf{0}) \neq 0$ for $k \to 0$. This is true for any $\mu_I \neq \mu_I^*$.

Fig. 13 shows the flow of u_ϕ in three dimensions for different values of $(n^{1/3} a_{BI})^{-1}$ at the corresponding ground state energies μ_I^*. This coupling saturates to finite values. However, we observe that u_ϕ saturates to values closer to
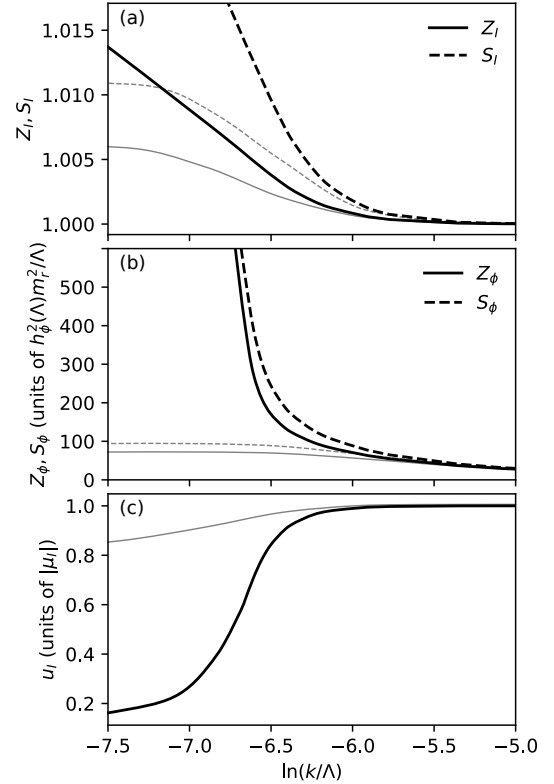
FIG. 12. Renormalization group flows in three dimensions at unitarity $a_{BI}^{-1} = 0$ for $n^{1/3} a_{BB} = 3.5 \times 10^{-3}$. The black lines correspond to flows at the ground state energy $\mu_I^* < 0$ such that $q_{0,\pm}^* \to 0$ (36) for $k \to 0$. The thin gray linse correspond to an energy $\mu_I < \mu_I^*$.

zero as $(n^{1/3} a_{BI})^{-1}$ increases. Our interpretation is that this signals the polaron-to-molecule crossover. As we increase the boson-impurity interaction, the molecule state dominates, and so the dimer self-energy in vacuum u_ϕ decreases. Analogous flows are obtained in two dimensions.

We stress that the coupling u_I can not be identified as the impurity self energy in vacuum because it contains the effect of the higher order couplings λ_{BI} and
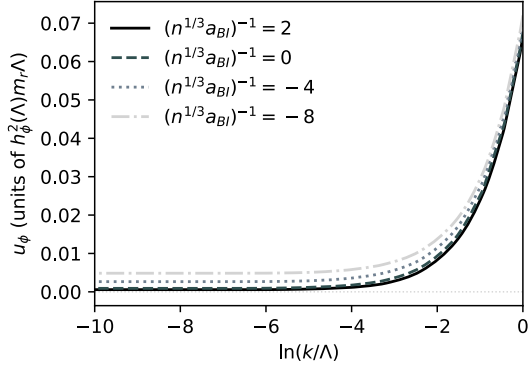
FIG. 13. Renormalization group flow of u_ϕ in three dimensions for different boson-impurity scattering lengths a_{BI} for $n^{1/3}a_{BB} = 3.5 \times 10^{-3}$. All the lines correspond to flow at the corresponding ground state energy μ_I^*.

λ_{BII} (which have been eliminated from the flow). Therefore, we do not observe a change in u_I for different $(n^{1/3}a_{BI})^{-1}$.

Appendix C: Estimation of the effective mass in the repulsive branch

Because in the DE we follow the flow at zero momentum, we can not compute the complete Green's function $G(q)$, and therefore we can not extract quantities such as the effective mass and the residue [25]. However, here we propose a way to estimate the effective mass in the repulsive branch, which can give us an idea of how the FRG could perform with a more robust calculation.

From the pole (15), we can naively impose at $k = 0$ that

$$\frac{\mathbf{q}^2}{2m_I^*} = \frac{1}{S_I}\left(Z_I\frac{\mathbf{q}^2}{2m_I} + u_I\right), \qquad \text{(C1)}$$

where m_I^* is the estimated effective mass, in analogy to a rigorous definition [25]. At the physical ground state energy μ_I^*, we have that $u_I = 0$. This gives the following expression

$$\frac{m_I^*}{m_I} = \frac{S_I}{Z_I}\bigg|_{k=0}, \qquad \text{(C2)}$$

which enables us to extract the effective mass in the repulsive branch. An analogous condition was proposed in Ref. [101] to extract effective masses with the FRG in a Bose-Hubbard model.

Fig. 14 shows effective masses in three dimensions for equal boson and impurity masses. We compare with the

perturbative solution for $m_B = m_I$ [102]

$$\frac{m_I^*}{m_I} = 1 + \frac{64}{45\sqrt{\pi}}\sqrt{na_{BB}^3}\frac{a_{BI}^2}{a_{BB}^2}, \qquad \text{(C3)}$$

which was shown to give a good description compared to more sophisticated approaches [45]. Our estimate is in good agreement with the perturbative solution, showing the correct trend.

Fig. 15 shows effective masses in two dimensions for equal boson and impurity masses. We compare with MC simulations from Ref. [48], and with the perturbative LHY-type solution for $m_B = m_I$ [48]

$$\frac{m_I^*}{m_I} = 1 + \frac{1}{2}\frac{\ln(n^{1/2}a_{BB})}{\ln^2(n^{1/2}a_{BI})}. \qquad \text{(C4)}$$

We obtain a reasonable agreement again with the perturbative solution and the MC results, especially with the latter. This suggests that, even within our approximation, the FRG is able to give a good description of the effective mass.

We are not able to provide a similar expression in the attractive branch where the poles have a much more complicated structure. Furthermore, because the impurity and dimer degrees of freedom are hybridized, the calculation of the effective mass is even less straightforward. We expect that in future work, we will be able to provide an accurate description by including the momentum dependence of the couplings.
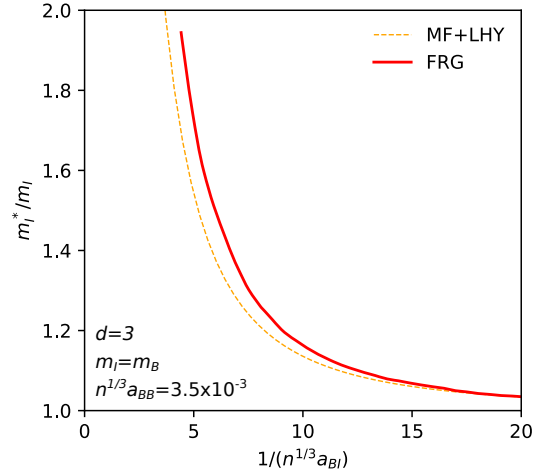

FIG. 14. Effective mass m_I^*/m_I of the repulsive branch in three dimensions as a function of $(n^{1/3}a_{BI})^{-1}$ for $m_B = m_I$ and $n^{1/3}a_{BB} = 3.5 \times 10^{-3}$. The solid red line corresponds to FRG calculations, whereas the dashed orange line to the perturbative solution (C3).

[1] L. Landau and S. Pekar, Zh. Eksp. Teor. Fiz **18**, 419 (1948).

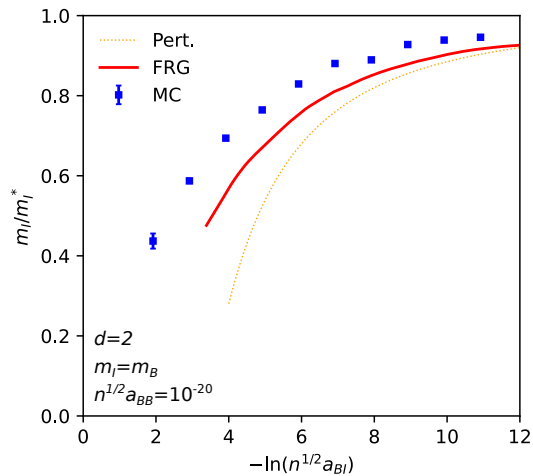[2] A. Fabrocini, S. Fantoni, S. Rosati, and A. Polls, Phys-

FIG. 15. Effective mass m_I^*/m_I of the repulsive branch in two dimensions as a function of $-\ln(n^{1/2}a_{BI})$ for $m_B = m_I$ and $n^{1/2}a_{BB} = 10^{-20}$. The solid red line corresponds to FRG calculations, the blue squares to MC simulations [48], and the dashed orange line to the perturbative solution (C4).

ical Review B **33**, 6057 (1986).

[3] A. Fabrocini and A. Polls, Physical Review B **58**, 5209 (1998).

[4] A. S. Alexandrov and J. T. Devreese, *Advances in polaron physics* (Springer, Berlin, 2010).

[5] A. Schirotzek, C.-H. Wu, A. Sommer, and M. W. Zwierlein, Physical Review Letters **102**, 230402 (2009).

[6] S. Nascimbène, N. Navon, K. J. Jiang, L. Tarruell, M. Teichmann, J. McKeever, F. Chevy, and C. Salomon, Physical Review Letters **103**, 170402 (2009).

[7] C. Kohstall, M. Zaccanti, M. Jag, A. Trenkwalder, P. Massignan, G. M. Bruun, F. Schreck, and R. Grimm, Nature (London) **485**, 615 (2012).

[8] P. Massignan, M. Zaccanti, and G. M. Bruun, Rep. Prog. Phys. **77**, 034401 (2014).

[9] J. Levinsen and M. M. Parish, "Strongly interacting two-dimensional fermi gases," in *Annual Review of Cold Atoms and Molecules* (2015) Chap. 1, pp. 1–75.

[10] M. Cetina, M. Jag, R. S. Lous, J. T. M. Walraven, R. Grimm, R. S. Christensen, and G. M. Bruun, Physical Review Letters **115**, 135302 (2015).

[11] M. Cetina, M. Jag, R. S. Lous, I. Fritsche, J. T. M. Walraven, R. Grimm, J. Levinsen, M. M. Parish, R. Schmidt, M. Knap, and E. Demler, Science **354**, 96 (2016).

[12] F. Scazza, G. Valtolina, P. Massignan, A. Recati, A. Amico, A. Burchianti, C. Fort, M. Inguscio, M. Zaccanti, and G. Roati, Physical Review Letters **118**, 083602 (2017).

[13] N. Darkwah Oppong, L. Riegger, O. Bettermann, M. Höfer, J. Levinsen, M. M. Parish, I. Bloch, and S. Fölling, Physical Review Letters **122**, 193604 (2019).

[14] G. Ness, C. Shkedrov, Y. Florshaim, O. K. Diessel, J. von Milczewski, R. Schmidt, and Y. Sagi, Phys. Rev. X **10**, 041019 (2020).

[15] H. S. Adlong, W. E. Liu, F. Scazza, M. Zaccanti, N. D. Oppong, S. Fölling, M. M. Parish, and J. Levinsen, Physical Review Letters **125**, 133401 (2020).

[16] I. Fritsche, C. Baroni, E. Dobler, E. Kirilov, B. Huang, R. Grimm, G. M. Bruun, and P. Massignan, Physical Review A **103**, 053314 (2021).

[17] I. Bloch, J. Dalibard, and W. Zwerger, Reviews of Modern Physics **80**, 885 (2008).

[18] J. Catani, G. Lamporesi, D. Naik, M. Gring, M. Inguscio, F. Minardi, A. Kantian, and T. Giamarchi, Physical Review A **85**, 023623 (2012).

[19] N. B. Jørgensen, L. Wacker, K. T. Skalmstang, M. M. Parish, J. Levinsen, R. S. Christensen, G. M. Bruun, and J. J. Arlt, Physical Review Letters **117**, 055302 (2016).

[20] M.-G. Hu, M. J. Van de Graaff, D. Kedar, J. P. Corson, E. A. Cornell, and D. S. Jin, Physical Review Letters **117**, 055301 (2016).

[21] Z. Z. Yan, Y. Ni, C. Robens, and M. W. Zwierlein, Science **368**, 190 (2020).

[22] G. E. Astrakharchik and L. P. Pitaevskii, Physical Review A **70**, 013608 (2004).

[23] J. Tempere, W. Casteels, M. K. Oberthaler, S. Knoop, E. Timmermans, and J. T. Devreese, Physical Review B **80**, 184504 (2009).

[24] J. Levinsen, M. M. Parish, R. S. Christensen, J. J. Arlt, and G. M. Bruun, Physical Review A **96**, 063622 (2017).

[25] S. P. Rath and R. Schmidt, Physical Review A **88**, 053632 (2013).

[26] A. Camacho-Guardian and G. M. Bruun, Physical Review X **8**, 031042 (2018).

[27] V. Pastukhov, Journal of Physics B: Atomic, Molecular and Optical Physics **51**, 155203 (2018).

[28] V. Pastukhov, Journal of Physics A: Mathematical and Theoretical **51**, 195003 (2018).

[29] N.-E. Guenther, P. Massignan, M. Lewenstein, and G. M. Bruun, Physical Review Letters **120**, 050405 (2018).

[30] P. Massignan, C. J. Pethick, and H. Smith, Phys. Rev. A **71**, 023606 (2005).

[31] W. Li and S. Das Sarma, Physical Review A **90**, 013618 (2014).

[32] J. Levinsen, M. M. Parish, and G. M. Bruun, Physical Review Letters **115**, 125302 (2015).

[33] Y. E. Shchadilova, R. Schmidt, F. Grusdt, and E. Demler, Physical Review Letters **117**, 113002 (2016).

[34] S. M. Yoshida, S. Endo, J. Levinsen, and M. M. Parish, Physical Review X **8**, 011024 (2018).

[35] A. S. Dehkharghani, A. G. Volosniev, and N. T. Zinner, Physical Review Letters **121**, 080405 (2018).

[36] M. Drescher, M. Salmhofer, and T. Enss, Physical Review A **99**, 023601 (2019).

[37] N.-E. Guenther, R. Schmidt, G. M. Bruun, V. Gurarie, and P. Massignan, Physical Review A **103**, 013317 (2021).

[38] P. Massignan, N. Yegovtsev, and V. Gurarie, Physical Review Letters **126**, 123403 (2021).

[39] L. A. Peña Ardila, Physical Review A **103**, 033323 (2021).

[40] J. Levinsen, L. A. P. Ardila, S. M. Yoshida, and M. M. Parish, Phys. Rev. Lett. **127**, 033401 (2021).

[41] R. Schmidt and T. Enss, arXiv:2102.13616 (2021).

[42] F. Grusdt, Y. E. Shchadilova, A. N. Rubtsov, and E. Demler, Scientific Reports **5**, 12124 (2015).

[43] F. Grusdt, R. Schmidt, Y. E. Shchadilova, and E. Demler, Physical Review A **96**, 013607 (2017).

[44] T. Ichmoukhamedov and J. Tempere, Physical Review

A **100**, 043605 (2019).

[45] L. A. P. Peña Ardila and S. Giorgini, Physical Review A **92**, 033612 (2015).

[46] L. A. P. Peña Ardila and S. Giorgini, Physical Review A **94**, 063640 (2016).

[47] L. A. Peña Ardila, N. B. Jørgensen, T. Pohl, S. Giorgini, G. M. Bruun, and J. J. Arlt, Physical Review A **99**, 063607 (2019).

[48] L. A. P. Peña Ardila, G. E. Astrakharchik, and S. Giorgini, Physical Review Research **2**, 023405 (2020).

[49] G. Pascual and J. Boronat, arXiv:2105.07738 (2021).

[50] C. Wetterich, Physics Letters B **301**, 90 (1993).

[51] J. Berges, N. Tetradis, and C. Wetterich, Physics Reports **363**, 223 (2002).

[52] N. Dupuis, L. Canet, A. Eichhorn, W. Metzner, J. Pawlowski, M. Tissier, and N. Wschebor, Physics Reports **910**, 1 (2021).

[53] S. Moroz, S. Floerchinger, R. Schmidt, and C. Wetterich, Physical Review A **79**, 042705 (2009).

[54] S. Floerchinger, R. Schmidt, S. Moroz, and C. Wetterich, Physical Review A **79**, 013603 (2009).

[55] S. Floerchinger, S. Moroz, and R. Schmidt, Few-Body Systems **51**, 153 (2011).

[56] R. Schmidt and S. Moroz, Physical Review A **81**, 052709 (2010).

[57] B. Jaramillo Ávila and M. C. Birse, Physical Review A **88**, 043613 (2013).

[58] B. Jaramillo Ávila and M. C. Birse, Physical Review A **92**, 023601 (2015).

[59] Y. Horinouchi and M. Ueda, Physical Review A **94**, 050702(R) (2016).

[60] M. C. Birse, B. Krippa, J. A. McGovern, and N. R. Walet, Physics Letters B **605**, 287 (2005).

[61] S. Diehl and C. Wetterich, Physical Review A **73**, 033615 (2006).

[62] S. Diehl and C. Wetterich, Nuclear Physics B **770**, 206 (2007).

[63] S. Floerchinger, M. Scherer, S. Diehl, and C. Wetterich, Physical Review B **78**, 174528 (2008).

[64] S. Floerchinger, M. M. Scherer, and C. Wetterich, Physical Review A **81**, 063619 (2010).

[65] S. Diehl, S. Floerchinger, H. Gies, J. Pawlowkski, and C. Wetterich, Annalen der Physik **522**, 615 (2010).

[66] I. Boettcher, J. M. Pawlowski, and C. Wetterich, Physical Review A **89**, 053630 (2014).

[67] I. Boettcher, J. Braun, T. K. Herbst, J. M. Pawlowski, D. Roscher, and C. Wetterich, Physical Review A **91**, 013610 (2015).

[68] B. M. Faigle-Cedzich, J. M. Pawlowski, and C. Wetterich, Physical Review A **103**, 033320 (2021).

[69] R. Schmidt and T. Enss, Physical Review A **83**, 063620 (2011).

[70] K. Kamikado, T. Kanazawa, and S. Uchino, Physical Review A **95**, 013612 (2017).

[71] J. von Milczewski, F. Rose, and R. Schmidt, arXiv:2104.14017 (2021).

[72] N. Dupuis and K. Sengupta, Europhysics Letters **80**, 50007 (2007).

[73] C. Wetterich, Physical Review B **77**, 064504 (2008).

[74] S. Floerchinger and C. Wetterich, Physical Review A **77**, 053603 (2008).

[75] S. Floerchinger and C. Wetterich, Physical Review A **79**, 013601 (2009).

[76] N. Dupuis, Physical Review A **80**, 043627 (2009).

[77] F. Isaule, M. C. Birse, and N. R. Walet, Annals of Physics **412**, 168006 (2020).

[78] F. Isaule, I. Morera, A. Polls, and B. Juliá-Díaz, Physical Review A **103**, 013318 (2021).

[79] J.-P. Blaizot, R. M. Galain, and N. Wschebor, Europhysics Letters **72**, 705 (2005).

[80] D. F. Litim, Physics Letters B **486**, 92 (2000).

[81] L. Viverit and S. Giorgini, Physical Review A **66**, 063604 (2002).

[82] R. S. Christensen, J. Levinsen, and G. M. Bruun, Physical Review Letters **115**, 160401 (2015).

[83] R. Desbuquois, L. Chomaz, T. Yefsah, J. Léonard, J. Beugnon, C. Weitenberg, and J. Dalibard, Nature Physics **8**, 645 (2012).

[84] C.-L. Hung, X. Zhang, N. Gemelke, and C. Chin, Nature **470**, 236 (2011).

[85] A. Rançon and N. Dupuis, Physical Review A **85**, 063607 (2012).

[86] N. N. Khuri, A. Martin, J.-M. Richard, and T. T. Wu, Journal of Mathematical Physics **50**, 072105 (2009).

[87] A. Galea, T. Zielinski, S. Gandolfi, and A. Gezerlis, Journal of Low Temperature Physics **189**, 451 (2017).

[88] M. C. Birse, Physical Review C **77**, 047001 (2008).

[89] C. Chin, R. Grimm, P. Julienne, and E. Tiesinga, Reviews of Modern Physics **82**, 1225 (2010).

[90] L. Tanzi, C. R. Cabrera, J. Sanz, P. Cheiney, M. Tomza, and L. Tarruell, Phys. Rev. A **98**, 062712 (2018).

[91] B. Field, J. Levinsen, and M. M. Parish, Physical Review A **101**, 013623 (2020).

[92] M. Sun, H. Zhai, and X. Cui, Physical Review Letters **119**, 013401 (2017).

[93] H.-W. Hammer and D. T. Son, Physical Review Letters **93**, 250408 (2004).

[94] L.-C. Ha, C.-L. Hung, X. Zhang, U. Eismann, S.-K. Tung, and C. Chin, Physical Review Letters **110**, 145302 (2013).

[95] P. Christodoulou, M. Gałka, N. Dogra, R. Lopes, J. Schmitt, and Z. Hadzibabic, Nature **594**, 191 (2021).

[96] T. Machado and N. Dupuis, Physical Review E **82**, 041128 (2010).

[97] A. Rançon and N. Dupuis, Physical Review B **83**, 172501 (2011).

[98] A. Muñoz de las Heras, E. Macaluso, and I. Carusotto, Physical Review X **10**, 041058 (2020).

[99] T. Graß, B. Juliá-Díaz, N. Baldelli, U. Bhattacharya, and M. Lewenstein, Physical Review Letters **125**, 136801 (2020).

[100] D. Pimenov, A. Camacho-Guardian, N. Goldman, P. Massignan, G. M. Bruun, and M. Goldstein, Physical Review B **103**, 245106 (2021).

[101] A. Rançon and N. Dupuis, Physical Review A **85**, 011602(R) (2012).

[102] F. M. Cucchietti and E. Timmermans, Physical Review Letters **96**, 210401 (2006).